Stereodivergent Synthesis of Enantiopure Oligomers with Tailored Physical Properties

Guofeng Li,[1,2,#] Zixuan Huang,[1,#] Benjamin B. Noble,[3] Donald S. Thomas,[4] Yingying Chu,[1] Ruizhe Liu,[1] Lei Zhang,[1] Kotaro Satoh,[5] Masami Kamigaito,[6] Michelle L. Coote,[7] Xing Wang,[2,*] and Jiangtao Xu[1,*]

[1]Centre for Advanced Macromolecular Design and Australian Centre for NanoMedicine, School of Chemical Engineering, UNSW Sydney, NSW 2052, Australia

[2]Beijing Advanced Innovation Center for Soft Matter Science and Engineering, Beijing Laboratory of Biomedical Materials, Beijing University of Chemical Technology, Beijing 100029, P. R. China

[3]School of Engineering, STEM College, RMIT University, VIC 3000, Australia

[4]Nuclear Magnetic Resonance Facility, Mark Wainwright Analytical Centre, UNSW Sydney, NSW 2052, Australia

[5]Department of Chemical Science and Engineering, School of Materials and Chemical Technology, Tokyo Institute of Technology, Ookayama, Meguro-ku, Tokyo 152-8550, Japan

[6]Department of Molecular and Macromolecular Chemistry, Graduate School of Engineering, Nagoya University, Furo-cho, Chikusa-ku, Nagoya 464-8603, Japan

[7]Research School of Chemistry, Australian National University, Canberra, ACT 2601, Australia

ABSTRACT

Stereochemistry can significantly affect the chemical and physical properties of synthetic polymers. Compared to the structural precision of natural biomacromolecules (e.g. proteins and nucleic acids) that are chiral and enantiopure, fully controlling the stereochemistry of synthetic polymers is considerably more challenging. However, the development of next generation polymer materials will require increasing levels of microstructural control and an in-depth understanding of structure-property relationships. Herein, we assemble an unprecedented library of enantiopure oligomers, specifically indene-maleimide-indene trimers, with identical primary structure but different stereochemistry through a novel highly stereoselective radical addition process. Full characterization of these unique trimers reveals that the structural rigidity and molecular compactness are responsible for their unique physical properties, including crystallization, glass transition temperature and optical activity. This strategy provides an innovative means to build oligomeric blocks for synthetic polymers and tailor their physical properties.

INTRODUCTION

One of the 'signatures of life' is that the building blocks of natural biopolymers (e.g. *L*-amino acids and *D*-sugars) are homochiral,[1] which illustrates the critical importance of stereochemistry in regulating their structures, properties and functions.[2-4] For instance, the double helix structure of DNA, which is governed by supramolecular hydrogen bonding, requires *D*-form deoxyribose sugar units within the component phosphate backbones. The impact of stereochemistry on physical properties are well-known in natural rubber and gutta-percha as two isomers (*cis* and *trans*) of high molecular weight polyisoprene, with natural rubber being elastic but gutta-percha being hard and brittle. In synthetic polymers, stereochemistry has also been recognized to significantly affect the physical properties since the discovery of synthetic isotactic polypropylene in 1955.[5] For instance, isotactic polystyrene is semicrystalline (with 60% crystallinity and $T_m \approx 250$ °C) and has improved mechanical properties relative to amorphous atactic polystyrene.[6]

Recent advances in polymer synthesis have largely focused on controlling sequence and chain length.[7-27] These resulting monodisperse and sequence-defined oligomers/polymers possess intriguing properties that are comparable to natural biomacromolecules.[4, 17, 28] However, while natural biomacromolecules are chiral and enantiopure, synthetic oligomers/polymers are usually much less structurally precise. Fully controlling the absolute stereochemistry is the ultimate goal of macromolecular synthesis, as it would enable access to vastly more synthetic materials with interesting properties that could surpass natural polymers. While stereochemistry is known to significantly influence macroscopic properties, detailed investigations on stereostructure-property relationships are rare because of the lack of effective synthetic methodologies to access such control.[19] With conventional polymers, *diastereocontrol* (also known as tacticity control) can usually be regulated by asymmetric or stereoselective polymerization in a chain-growth manner (e.g. coordination, ionic or radical polymerization), mostly in the presence of chiral catalysts or other additives.[29-34] Monodisperse oligomers/polymers can be obtained by chromatography separation of such tactic polymers.[35-36] However, approaches for the synthesis of *enantiocontrolled* polymers with defined chain length

are relatively limited, with perhaps the only well-known example being solid-phase peptide or oligonucleotide synthesis. Other methods have involved direct condensation of chiral monomers through iterative growth[19-20, 37-41] and successive monomer addition[42] in solution or on solid support, which indicates limited cases of success. Additionally, the chiral monomers have been confined to α,ω-heterodifunctional monomers such as lactic acid and similar structures as amino acids, which mostly requires tedious manipulation of protection and deprotection on functional groups during synthesis. Therefore, it is of paramount importance to develop innovative methodologies for the robust synthesis from broad monomer scope (e.g. vinyl monomers) to increase stereostructural diversity of such enantiopure macromolecules. The investigation of structure-property relationship would enable access to next generation of polymer materials.

Recently, we developed a methodology of photoinduced-reversible addition-fragmentation chain transfer single unit monomer insertion (RAFT SUMI) to iteratively insert two cyclic electron-donor/acceptor vinyl monomers, indene and maleimide, into a trithiocarbonate to prepare sequence-defined oligomers.[43-44] A simplified process as depicted in **Figure 1a** starts with radical generation (R•) from a RAFT agent (R-SCSZ) through visible light catalysis. This transient radical subsequently undergoes a single unit monomer addition to form an adduct radical followed by carbon-thiocarbonylthio coupling to generate the SUMI product. Crucially, the insertion of cyclic monomers proceeds in a highly *trans*-selective manner within monomer units along the backbone due to steric hindrance. This stereoselectivity inspires us to further control the absolute stereochemistry (enantiocontrol) of oligomers as natural biomacromolecules do, which is considered as an extreme challenge in radical chemistry.[45] With this in mind, in this study we drew inspiration from the use of chiral monomers in nature, introducing asymmetric substituents within cyclic vinyl monomers (indene) to induce stereoselective radical addition to precisely prepare enantiopure oligomers with diverse stereochemical configurations. These enantiopure oligomers present divergent physical properties that correlate to their unique stereochemical structures.

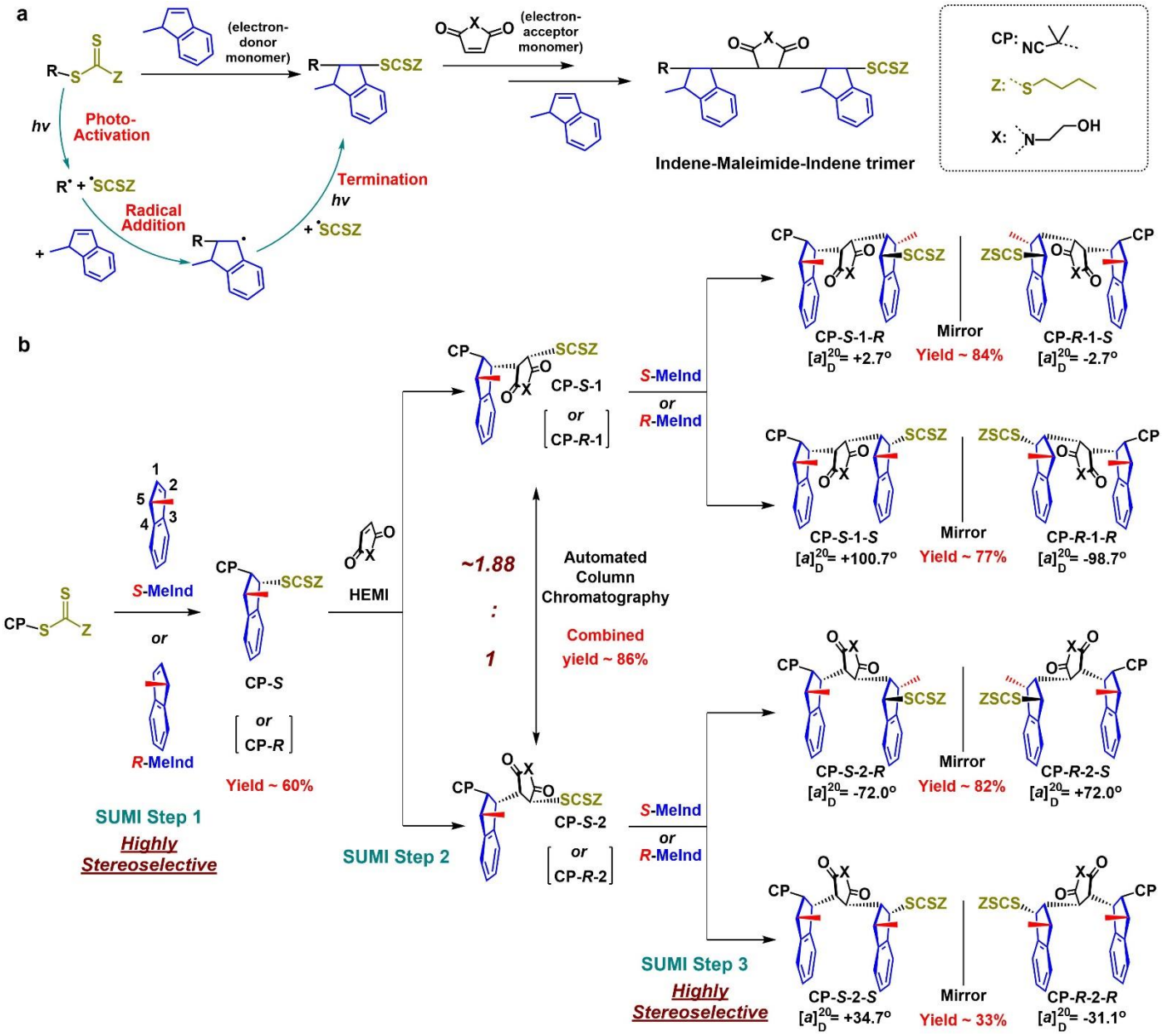

Figure 1. Stereodivergent synthesis of enantiopure isomeric trimers through a highly stereoselective photoinduced reversible addition-fragmentation chain transfer single unit monomer insertion (photo-RAFT SUMI) process. **a)** Successive photo-RAFT SUMI process and its simplified mechanism including photo-activation, radical addition, and termination by carbon-thiocarbonylthio radical coupling. For clarity, the RAFT processes are not specified. **b)** Three-step synthesis and stereochemistry of eight enantiopure trimers investigated in this study. The yield means the isolated yield of the SUMI product for each step.

RESULTS AND DISCUSSION

1. Stereodivergent synthesis of enantiopure oligomers

A chiral analogue of indene that possesses an alkyl substitute on the 5-position, *S*-MeInd and *R*-MeInd, was synthesized (**Figure 1b)** from their respective propionic acids followed by Friedel-Craft acylation,[46] $NaBH_4$ reduction[47] and elimination reactions.[48] Each chiral monomer can be stereoselectively inserted into a trithiocarbonate (2-cyanopropan-2-yl butyl trithiocarbonate, CPBTC), which leads to the highly diastereoselective adduct with a *trans-trans* configuration only, instead of the three other possible configurations (*trans-cis* (ii), *cis-trans* (iii) and *cis-cis* (iv) as depicted in **Figure 2a**). This is attributed to the proximity of the methyl substituent in *S*-MeInd to the double-bond, which effectively prevents *cis* addition of an incoming radical to the 1-position carbon and allows the formation of the *trans* adduct radical exclusively. Subsequently, a selective *trans* coupling of thiocarbonylthio radical with the adduct radical occurs to form SUMI product CPBTC-MeInd$_{(S)}$ (denoted as **CP-*S***).[43]

Both NMR spectroscopy and quantum chemical calculations unambiguously establish the *trans-trans* stereochemistry of the product **CP-*S***. In ^{1}H NMR spectrum for the reaction mixture of CPBTC with *S*-MeInd (Supplementary **Figure 1**), signals corresponding to a single diastereomer (assigned to **CP-*S***) are observed. Meanwhile, density functional theory calculations clearly reveal that the *trans-trans* configuration of a **CP-*S*** model possesses the lowest Gibbs free energy by at least 17 kJ/mol compared with the other three configurations (**Figure 2a**). Similarly, CPBTC-MeInd$_{(R)}$ (denoted as **CP-*R***) was synthesized using *R*-MeInd to react with CPBTC, generating only the *trans-trans* configuration. Significantly, chiral HPLC analysis (Supplementary **Figure 2**) demonstrated enantiomeric excess (*ee*) values > 99% for both enantiopure mono-adducts indicating no racemization during the reaction, highlighting the robustness of this synthetic method.

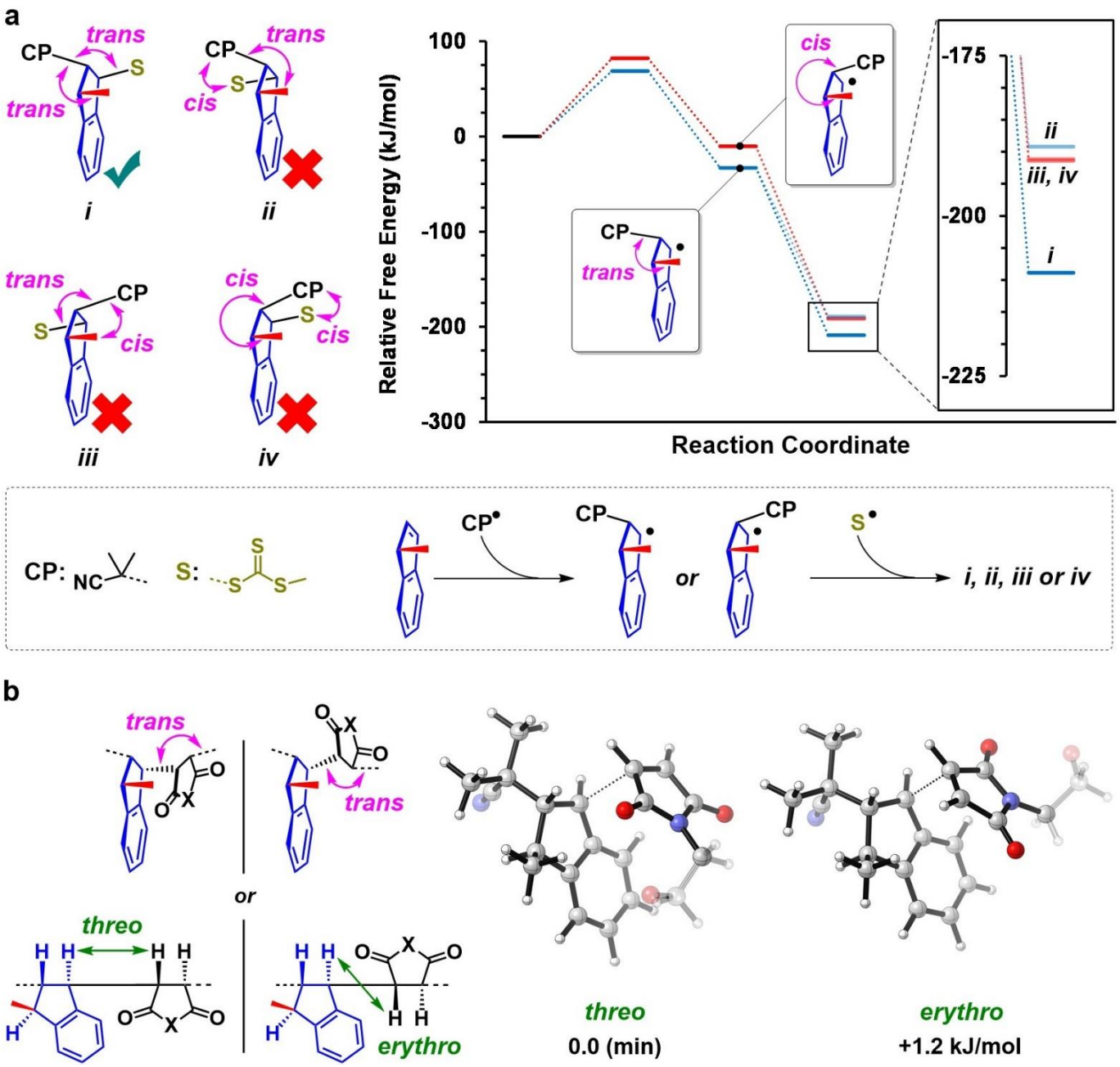

Figure 2. Stereoselectivity of the radical addition steps during a photo-RAFT SUMI process. a) Density functional theory calculations of the relative Gibbs free energies (298 K, DMSO) of four possible stereoisomeric SUMI adducts and their transition states from the insertion reaction of *S*-MeInd into a RAFT agent. The butyl tail in CPBTC was truncated to a methyl substituent to simplicity. **b)** Two stereo-configurations (*threo* and *erythro*) of CPBTC-MeInd$_{(S)}$-HEMI (left) and the relative Gibbs free energy difference for the respective transition states of HEMI insertion into a CP-*S* radical (right).

The synthesized **CP-*S*** (or **CP-*R***) was then employed as a chiral macro-RAFT agent for further chain-

growth by inserting a maleimide monomer, *N*-hydroxylethyl maleimide (HEMI) (**Figure 1b**). Since HEMI is a symmetric monomer, both *threo* and *erythro* structures can be formed during radical addition (**Figure 2b**). Fortunately, as the macro-RAFT, **CP-*S***, is enantiopure, the *threo* and *erythro* additions of HEMI only resulted in a mixture of two enantiopure diastereomers in the crude product that had a molar ratio of 1.88:1 confirmed by ^{1}H NMR analysis (Supplementary **Figure 3**). Density functional theory calculations of the respective transition states showed that the *threo* structure is more stable than the *erythro* (by 1.2 kJ/mol, **Figure 2b**). This energy difference results in a theoretically predicted molar ratio for the two configurations of 1.6:1, in good agreement with the experimental result. The crude mixture of these two diastereomers can be efficiently separated by column chromatography due to their distinct R_f values (Supplementary **Figure 4**), affording the enantiopure dimers CPBTC-MeInd$_{(S)}$-HEMI$_{(1)}$ (**CP-*S*-1**) and CPBTC-MeInd$_{(S)}$-HEMI$_{(2)}$ (**CP-*S*-2**) (the denotation of "**1**" implies the first fraction collected in column chromatography and "**2**" for the second fraction), with a combined isolated yield of 86%. By calculating weight ratio of the two fractions (1.7:1), we confirmed that **CP-*S*-1** is assigned to the *threo* structure and **CP-*S*-2** is the *erythro* structure. An analogous reaction harnessing *R*-MeInd allows the synthesis of CPBTC-MeInd$_{(R)}$-HEMI$_{(1)}$ (**CP-*R*-1**) and CPBTC-MeInd$_{(R)}$-HEMI$_{(2)}$ (**CP-*R*-2**). ^{1}H and ^{13}C NMR analysis for these four purified dimers demonstrated excellent diastereomer excess (*de*) values (>99%) and purity (Supplementary Section 5.2). Additionally, the specific optical rotation ($[\alpha]_D^{20}$) for these two pairs of enantiomers gave almost the same but opposite values, respectively (Supplementary **Table 3**).

Next, the synthesis of eight enantiopure trimers was accomplished by inserting *S*- or *R*-MeInd monomer into these four enantiopure dimers (**Figure 1b**). Taking the synthesis of CPBTC-MeInd$_{(S)}$-HEMI$_{(1)}$-MeInd$_{(R)}$ (**CP-*S*-1-*R***) as an example, the dimer **CP-*S*-1** reached nearly 100% conversion after 70 h irradiation. Only one group of proton signals was observed in ^{1}H NMR spectrum of the crude product (Supplementary **Figure 5**), indicating similar diastereoselectivity to the first SUMI step. The ^{1}H and ^{13}C NMR and ESI-MS analyses verify the chemical structure and high purity (>99%) of the final product **CP-*S*-1-*R*** after purification (**Figure**

3 and Supplementary Information, Section 5.2). The other seven enantiopure trimers could be synthesized under analogous conditions. Comparing the ^{1}H NMR spectra of the four pairs of diastereomeric trimers clearly shows diverging chemical shifts (e.g., H1 to H6 in **Figure 3a**), which is indicative of how their stereoconfiguration influences the resulting chemical environments.

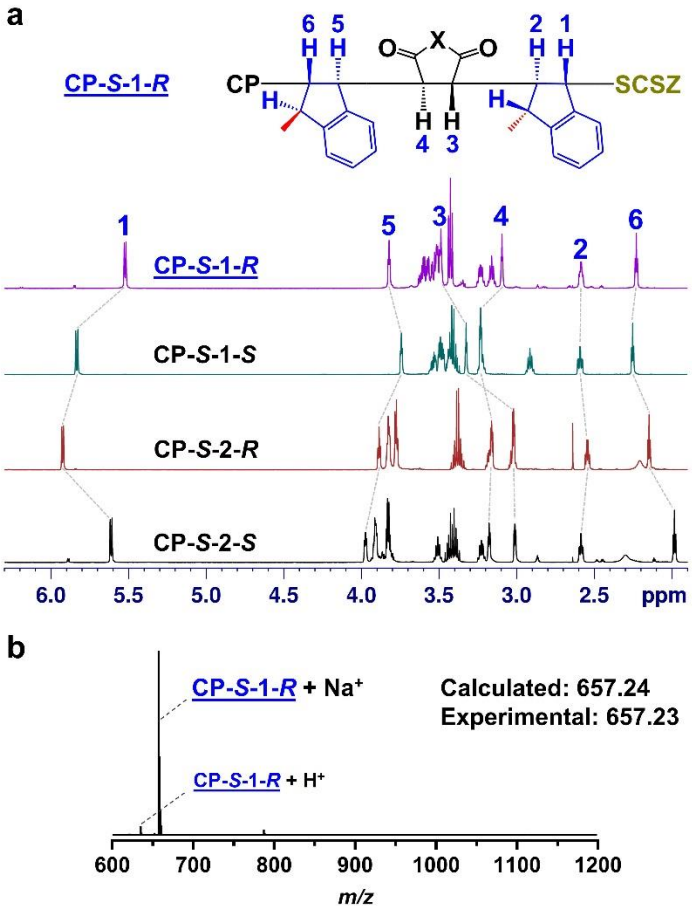

Figure 3. a) Comparison of ^{1}H NMR spectrum (δ 1.9-6.3 ppm) among four enantiopure trimers **CP-*S*-1-*R***, **CP-*S*-1-*S***, **CP-*S*-2-*R*** and **CP-*S*-2-*S***, showing significant differences in chemical shifts of corresponding protons (1 to 6) in the four trimers. **b)** ESI-MS analysis of **CP-*S*-1-*R***.

2. 3D models of enantiopure oligomers and their structural information

The stereostructures of eight synthetic trimers were confirmed by 2D NOESY NMR analysis that can accurately determine solution-phase molecular structures, particularly for peptides and nucleic acids, based on the interproton distance geometry.[49-50] Interproton distances can be obtained from the NOE cross-peak volumes. After the cross-peak volumes were calibrated, a table containing interproton distance constraints (<

2.5 Å, 2.5-4.5 Å, and 4.5-5 Å) was created for each trimer (Supplementary **Figures 6-9**). The full set of interproton distances were used to create constraints to generate a 3D molecular model (**Figure 4**), which provides access to the absolute stereochemical structures of the molecules consistent with our designations. This analysis also confirmed: (1) the stereochemistry of the original chiral monomer is preserved over the whole course of synthesis (i.e. no racemization occurred); (2) the *trans-trans* addition of each MeInd monomer was unambiguously verified; (3) the *threo* and *erythro* configurations of HEMI units in the trimers agree with the NMR and computational results in **Figure 2b**.

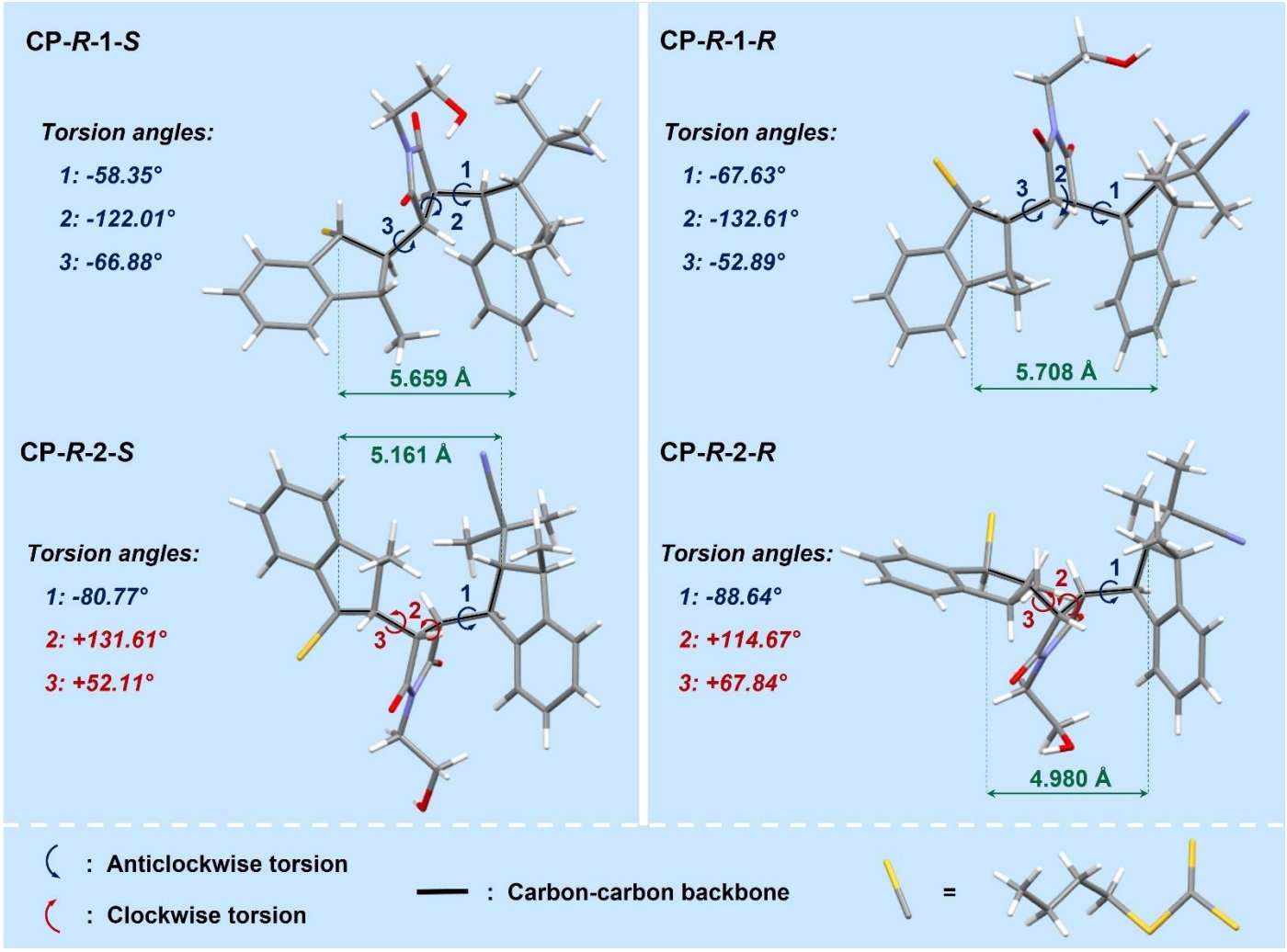

Figure 4. Capped stick 3D models of **CP-*R*-1-*S***, **CP-*R*-2-*S***, **CP-*R*-1-*R*** and **CP-*R*-2-*R*** established from 2D NOESY NMR analysis. C atom: grey; H: white; O: red; N: blue. *Note:* For clarity, the double bonds and CN triple bond are displayed as single bonds in the models. The 3D models were generated from the distance geometry simulation using interproton distances derived from NOESY spectra as constraints. More details are provided in the Supplementary Information.

These 3D models also provide detailed structural information, such as torsion angles and backbone lengths (the backbone is constituted by six chiral carbons in three monomer units). For instance, **CP-*R*-1-*S*** shows all anticlockwise torsions of the dihedral angles observed through CP side, whereas **CP-*R*-2-*S*** gives mixed torsions with both clockwise and anticlockwise. The backbone length of **CP-*R*-1-*S*** is much longer than **CP-*R*-2-*S*** (5.659 vs 5.161Å). Given the fact that the side chains of all monomer units in the **CP-*R*-1-*S*** and **CP-*R*-2-*S*** are the same, the different torsions and backbone lengths can be ascribed to distinct backbone stereochemistry (*threo* vs *erythro*) caused by two different connections of HEMI units in the molecules. The torsion angles and backbone lengths suggest the *erythro* configuration (**CP-*R*-2-*S***) adopts a more twisted and compact molecular conformation than *threo* (**CP-*R*-1-*S***). Similar behavior was observed for **CP-*R*-1-*R*** and **CP-*R*-2-*R***. Meanwhile, despite **CP-*R*-1-*S*** and **CP-*R*-1-*R*** being identical with respect to the first two units, the introduction of a divergent third unit (*S*-MeInd vs *R*-MeInd) significantly affected steric hindrance within the backbone, which can be observed from the respective torsion angles. Although such distortion has not much influence on the overall backbone lengths (5.659 Å vs 5.708 Å), these two trimers possess different stereochemistry in both their side chains and backbones. Bearing these general structural characteristics in mind, we sought to understand how the stereochemistry of these trimers influenced their physical properties including crystallization, thermal transitions (glass transition temperature, T_g) and optical properties.

3. Physical properties of synthetic enantiopure oligomers

Firstly, we investigated crystallization and T_g of these trimers in their bulk states using differential scanning calorimetry (DSC) (**Figure 5** and Supplementary **Figure 10**). As shown in **Figure 5a**, all four diastereomeric trimer pairs displayed typical polymeric characteristics with evident glass transitions in the range of 30~45 °C, despite their relatively low molecular weight (635 g/mol). However interestingly, only **CP-*R*-1-*S*** exhibited a cold crystallization transition[51] from 62 to 101 °C and an endothermic melting transition at 123 °C. The other three trimers did not show any transitions beyond T_g in both heating and cooling cycles.

This implies that **CP-*R*-1-S** is crystalline, while the other isomers adopt amorphous structures within their bulk solids. Additionally, by calculating the enthalpy changes of cold crystallization and melting for **CP-*R*-1-*S*** solid powder and its pure crystal (Supplementary **Figure 11**), we found that the initial **CP-*R*-1-*S*** powder is a semicrystalline oligomer composed of 41.7 wt% crystalline phase. The corresponding enantiomer, **CP-*S*-1-*R*** presented almost the same result (Supplementary **Figure 10**) with 39.7 wt% crystalline phase in its initial solid powder.

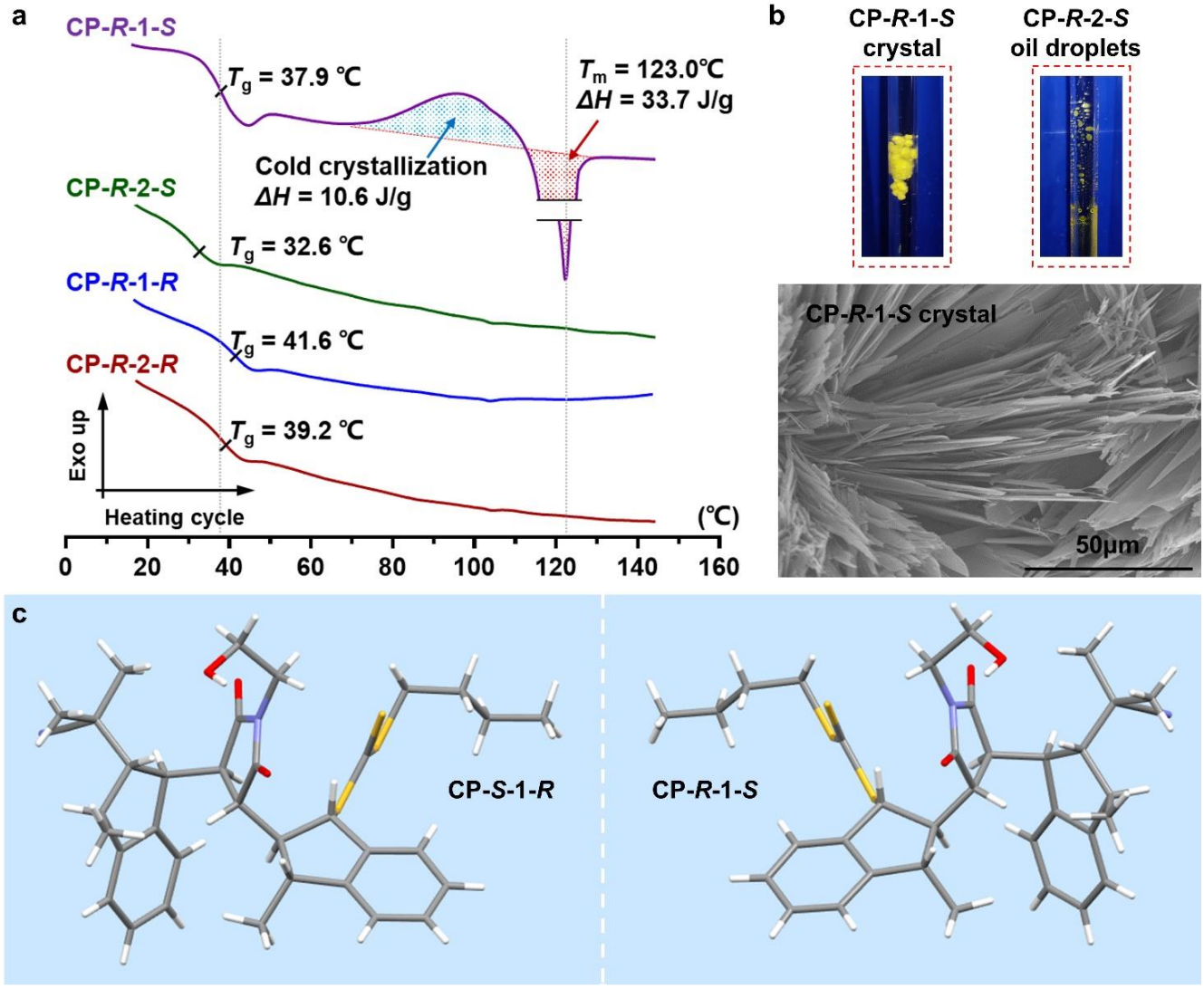

Figure 5. Thermal properties and crystallization behavior of enantiopure trimers. **a**) DSC curves of trimers **CP-*R*-1-*S***, **CP-*R*-2-*S***, **CP-*R*-1-*R*** and **CP-*R*-2-*R*** from 15 ºC to 145 ºC. **b)** Optical images (top) of **CP-*R*-1-*S*** crystals and **CP-*R*-2-*S*** oil droplets in recrystallization experiments, and SEM image (bottom) of **CP-*R*-1-*S*** crystals. **c)** Capped stick presentation of X-ray crystal structures of **CP-*S*-1-*R*** (left) and **CP-*R*-1-*S*** (right). For clarity, the double bonds and -CN triple bonds are displayed as single bonds.

This crystallization behavior was also verified by implementing two-solvent recrystallization of the trimers in various solvents (Supplementary **Tables 1** and **2**). **CP-*R*-1-*S*** (and **CP-*S*-1-*R***) formed needle-like fine crystals visualized by scanning electron microscopy (**Figure 5b** and Supplementary **Figures 12-13**), whereas other trimers precipitated in all tested solvents as oil droplets (**Figure 5b** and Supplementary **Figure 14**). DSC analysis on the collected crystals showed the presence of a melting transition at 123.0 ºC (T_m) and the absence of glass transitions (Supplementary, **Figure 11**), characteristic features of crystallization in small molecules. Taking advantage of this behavior, single crystals of **CP-*R*-1-*S*** (and **CP-*S*-1-*R***) were collected for X-ray diffraction (XRD) spectroscopy. The stereochemistry of the trimers was thus unambiguously validated (**Figure 5c** and Supplementary **Figure 15**), showing the mirror images between **CP-*R*-1-*S*** and **CP-*S*-1-*R***. Additionally, XRD results perfectly match the 3D models generated from 2D NOESY analysis (Supplementary **Figure 16**). The tendency of **CP-*R*-2-*S*** not to crystallize can be attributed to its more compact conformational structure, as discussed previously. Although **CP-*R*-1-*R*** has a comparable backbone length to **CP-*R*-1-*S***, it is more difficult to crystallize possibly due to its non-uniform structure.

Another intriguing feature illustrated in **Figure 5a** is the diverse T_g values of these oligomers, which highlights the remarkable impact of stereochemistry. Despite the rather low molecular weight of these oligomers (635 g/mol), there is an approximately 10 ºC difference between the lowest (**CP-*R*-2-*S***, 32.6 ºC) and the highest T_g values (**CP-*R*-1-*R***, 41.6 ºC). Comparing **CP-*R*-1-*S*** and **CP-*R*-2-*S***, which have the same side chain but different backbone stereochemistry, **CP-*R*-1-*S*** has a higher T_g than **CP-*R*-2-*S*** (37.9 ºC vs 32.6 ºC). Similarly, **CP-*R*-1-*R*** has a higher T_g than **CP-*R*-2-*R*** (41.6 ºC vs 39.2 ºC). These differences can be explained through their rigid molecular structures and unique stereochemical configurations.

The T_g of a polymer is affected by various molecular parameters including monomer structure and chain stiffness,[52-53] which can greatly influence the efficiency of molecular packing. Dense packing of polymer chains gives low free volume, decreased entropy and low translational mobility which is conducive to

increasing T_g.[53] This type of packing generally requires uniform and straight chain conformations, which result from the balance between the energetic cost for polymer chain bending and increased entropy.[54-55] That is, twisted or non-uniform macromolecular conformations provides loose packing of polymer chains and a low T_g. Building on this theory, **CP-*R*-2-*S*** and **CP-*R*-2-*R*** have more compact and twisted conformations than **CP-*R*-1-*S*** and **CP-*R*-1-*R*** (**Figure 4**) which causes looser molecular packing and consequently lower T_g values. We should note these 3D models were established from NMR data measured in solution, while the DSC analysis is performed in bulk. However, given the relative rigidity of these trimer structures comprised of three five member-ring monomers, difference in conformation between bulk and solution-phase should be relatively minor. These results clearly show stereochemistry can lead to dramatic changes in thermal properties of the bulk materials. The T_g difference between **CP-*R*-1-*S*** and **CP-*R*-1-*R*** (or **CP-*R*-2-*S*** and **CP-*R*-2-*R***) is more difficult to analyze because they possess different side chains in the third unit of monomers (*S*-MeInd vs *R*-MeInd). This affects stereochemistry in the backbone and steric hindrance with the nearby side chains. It is known that both the backbone and side chain of an oligomers/polymer can affect T_g, particularly for materials which possess both stiff backbones and side chains.[56]

The optical activity of these trimers is also affected by the stereochemistry as observed by their diverse specific rotations (Supplementary **Table 3**). For instance, although **CP-*S*-1-*R*** and **CP-*S*-2-*R*** have the same monomer structures, the backbone stereochemistry of the second monomer unit is different, which afford these two isomers distinct optical rotations (+2.7° vs -72°), demonstrating the backbone chirality has significant contribution to the optical activity of the whole molecule. Varied temperature circular dichroism (VT-CD) spectroscopy was also used to investigate optical properties based on the structural features of chiral molecules. In these synthetic trimers, the trithiocarbonate moiety that has an intense visible light absorption peaking at 436 nm (Supplementary **Figure 17a**) is an ideal achiral chromophore for investigating their optical behaviors under CD. As shown in **Figure 6**, the trithiocarbonate was successfully perturbed by the chiral trimers, leading to high quality CD signals in the range of 380 nm to 520 nm. Each pair of enantiomers (e.g. **CP-*R*-1-*S*** and

CP-*S*-1-*R* in **Figure 6a**) shows exact mirror images in their CD spectra. However, the four pairs of enantiomers presented distinct CD signal intensities and profiles, featuring their unique stereochemistry and molecular chirality. The trimer **CP-*R*-1-*S*** has the highest intensity and monosignate CD band, and the other two **CP-*R*-2-*S*** and **CP-*R*-2-*R*** have the lowest intensities and bisignate bands. **CP-*R*-2-*R*** presents characteristic positive couplet with a split CD spectrum, arising from the coupling interaction of thiocarbonylthio with another proximate chromophore (e.g. phenyl group) due to its compact molecular structure. As the temperature gradually increased from 273 K to 323 K, the CD signal intensity of **CP-*R*-1-*S*** decreased (**Figure 6a**), suggesting increased mobility of the whole molecule. In contrast, **CP-*R*-2-*S*** remained unchanged, which agrees with its rigid and compact structure as conveyed by its 3D model in **Figure 4**. This conclusion can also be drawn from the CD signal changes in **CP-*R*-1-*R*** and **CP-*R*-2-*R*** (**Figure 6b**). With increasing temperature, the decreasing CD intensities in **CP-*R*-1-*R*** is more evident than that in **CP-*R*-2-*R***. The exciton couplet in **CP-*R*-2-*R*** is slightly reduced but doesn't disappear, suggesting the coupling between chromophores is still strong due to molecular compactness. Additionally, the CD signals of the trimers are fully reversible over the temperature investigated (273~323 K), indicative of the high thermal stability of all molecules.

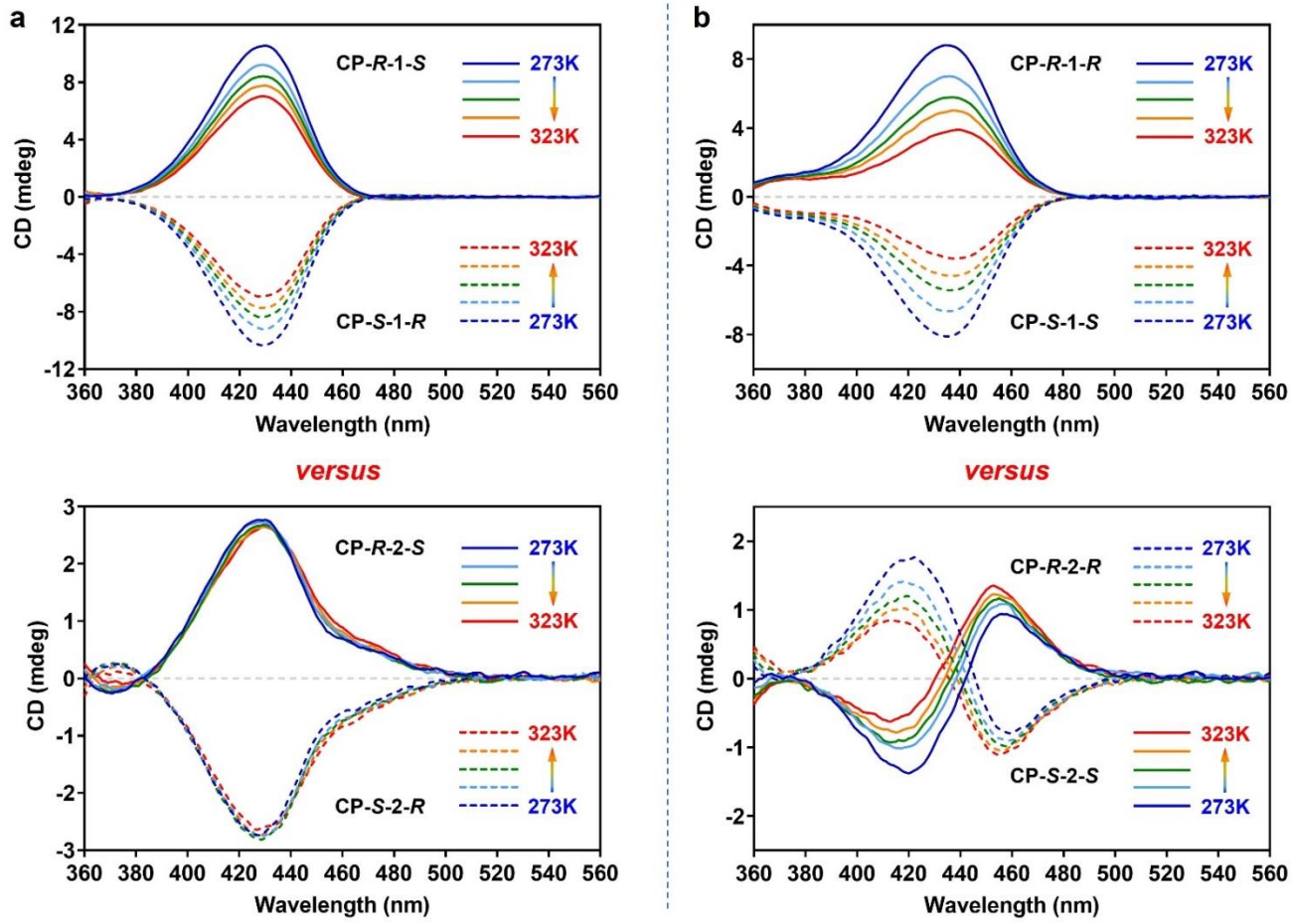

Figure 6. Varied temperature circular dichroism (VT-CD) spectra of eight enantiopure trimers. **a)** Comparison of **CP-*R*-1-*S***, **CP-*S*-1-*R***, **CP-*R*-2-*S***, and **CP-*S*-2-*R*** while increasing temperatures from 273 K to 323 K. **b)** Comparison of **CP-*R*-1-*R***, **CP-*S*-1-*S***, **CP-*R*-2-*R***, and **CP-*S*-2-*S*** while increasing temperatures from 273 K to 323 K.

CONCLUSIONS

In this article, we synthesized a novel library of enantiopure trimers by using a chiral substituent in a cyclic vinyl monomer to fully modulate their stereochemistry. Sequential highly diastereoselective radical addition reactions have been accomplished in a photo-RAFT SUMI process, producing eight enantiopure trimers with divergent stereochemistry. 2D NOESY analysis provides comprehensive structural information (molecular size and uniformity), which can be used to rationalize the physical properties of these trimers. Thermal analysis demonstrated that these trimers possess typical polymer characteristics with distinct glass transition temperatures. Among them, **CP-*R*-1-*S*/CP-*S*-1-*R*** are semicrystalline oligomers featuring superior

crystallization behavior, whereas the other isomers are amorphous. Given their inherent chirality, these trimers presented diversified optical rotations and CD signals in solution. With the temperature variation, the trimers of **CP-*R*-2-*S*/CP-*S*-2-*R*** and **CP-*R*-2-*R*/CP-*S*-2-*S*** displayed much less changes in CD than others due to their relatively compact molecular conformations. These results demonstrate stereochemical structure-property relationships for a novel class of monodisperse and optically active synthetic oligomers, illustrating how physical properties can be tailored by manipulating stereochemistry. The synthetic strategy provides an approach to precision oligomer synthesis through radical chain growth, but also for asymmetric polymerization using cyclic vinyl monomer and chirality induction. Meanwhile, the synthesized enantiopure oligomers can be used as building blocks to assemble enantiopure polymers with diverse structures and tailored properties.

ASSOCIATED CONTENT

Supporting information

The Supporting Information is available free of charge at https://pubs.acs.org/doi/***. Additional experimental details, materials and methods, including spectral characterization of the enantiopure molecules, raw computational data.

Notes

The authors declare no competing financial interest.

AUTHOR INFORMATION

Corresponding authors

wangxing@mail.buct.edu.cn (X.W.); j.xu@unsw.edu.au (J.X.)

Equal contribution

[#]G.L. and Z.H. contributed equally to this work.

ACKNOWLEDGEMENTS

J.X. acknowledges the Australian Research Council (ARC) for the financial support under the schemes of Future Fellowship (FT160100095). X.W. thanks the National Natural Science Foundation of China (21574008) and the Fundamental Research Funds for the Central Universities (BHYC1705B) of China for their financial support. Z.H. acknowledge Australian Research Training Program (RTP) for their PhD scholarship. M.L.C gratefully acknowledges a Georgina Sweet ARC Laureate Fellowship (FL170100041) and generous allocations of supercomputing time on the National Facility of the Australian National Computational Infrastructure. B.N. acknowledges Prof. Irene Yarovsky from RMIT University for supporting his participation in this project. Dr. Mohan Bhadbhade in Solid State and Elemental Analysis Unit, Mark Wainwright Analytical Centre at UNSW Sydney is acknowledged for the acquirement of single crystal X-ray data and the structure determination/refinement. J.X., M.K. and K.S. acknowledge Prof. Eiji Yashima from Nagoya University for the fruitful discussion on CD results and the valuable comments for the manuscript.

References

1. Blackmond, D. G., Autocatalytic Models for the Origin of Biological Homochirality. *Chem. Rev.* **2020,** *120*, 4831-4847.
2. Lutz, J.-F.; Lehn, J.-M.; Meijer, E. W.; Matyjaszewski, K., From Precision Polymers to Complex Materials and Systems. *Nat. Rev. Mater.* **2016,** *1*, 16024.
3. Rutten, M. G. T. A.; Vaandrager, F. W.; Elemans, J. A. A. W.; Nolte, R. J. M., Encoding Information into Polymers. *Nat. Rev. Chem.* **2018,** *2*, 365-381.
4. Lutz, J.-F.; Ouchi, M.; Liu, D. R.; Sawamoto, M., Sequence-Controlled Polymers. *Science* **2013,** *341*, 1238149.
5. Natta, G.; Pino, P.; Corradini, P.; Danusso, F.; Mantica, E.; Mazzanti, G.; Moraglio, G., Crystalline High Polymers of α-Olefins. *J. Am. Chem. Soc.* **1955,** *77*, 1708-1710.
6. Worch, J. C.; Prydderch, H.; Jimaja, S.; Bexis, P.; Becker, M. L.; Dove, A. P., Stereochemical Enhancement of Polymer Properties. *Nat. Rev. Chem.* **2019,** *3*, 514-535.
7. Lutz, J.-F., Defining the Field of Sequence-Controlled Polymers. *Macromol. Rapid Commun.* **2017,** *38*, 1700582.
8. De Neve, J.; Haven, J. J.; Maes, L.; Junkers, T., Sequence-Definition from Controlled Polymerization: The Next Generation of Materials. *Polym. Chem.* **2018,** *9*, 4692-4705.
9. Maron, E.; Swisher, J. H.; Haven, J. J.; Meyer, T. Y.; Junkers, T.; Börner, H. G., Learning from Peptides to Access Functional Precision Polymer Sequences. *Angew. Chem. Int. Ed.* **2019,** *58*, 10747-10751.
10. Xu, J., Single Unit Monomer Insertion: A Versatile Platform for Molecular Engineering through Radical Addition Reactions and Polymerization. *Macromolecules* **2019,** *52*, 9068-9093.
11. van Genabeek, B.; Lamers, B. A. G.; Hawker, C. J.; Meijer, E. W.; Gutekunst, W. R.; Schmidt, B. V. K. J., Properties and Applications of Precision Oligomer Materials; Where Organic and Polymer Chemistry Join Forces. *J. Polym. Sci.* **2021,** *59*, 373-403.

12. Lawrence, J.; Lee, S.-H.; Abdilla, A.; Nothling, M. D.; Ren, J. M.; Knight, A. S.; Fleischmann, C.; Li, Y.; Abrams, A. S.; Schmidt, B. V. K. J.; Hawker, M. C.; Connal, L. A.; McGrath, A. J.; Clark, P. G.; Gutekunst, W. R.; Hawker, C. J., A Versatile and Scalable Strategy to Discrete Oligomers. *J. Am. Chem. Soc.* **2016,** *138*, 6306-6310.

13. Martens, S.; Van den Begin, J.; Madder, A.; Du Prez, F. E.; Espeel, P., Automated Synthesis of Monodisperse Oligomers, Featuring Sequence Control and Tailored Functionalization. *J. Am. Chem. Soc.* **2016,** *138*, 14182-14185.

14. Holloway, J. O.; Mertens, C.; Du Prez, F. E.; Badi, N., Automated Synthesis Protocol of Sequence-Defined Oligo-Urethane-Amides Using Thiolactone Chemistry. *Macromol. Rapid Commun.* **2019,** *40*, 1800685.

15. Huang, Z.; Zhao, J.; Wang, Z.; Meng, F.; Ding, K.; Pan, X.; Zhou, N.; Li, X.; Zhang, Z.; Zhu, X., Combining Orthogonal Chain-End Deprotections and Thiol–Maleimide Michael Coupling: Engineering Discrete Oligomers by an Iterative Growth Strategy. *Angew. Chem. Int. Ed.* **2017,** *56*, 13612-13617.

16. Ji, Y.; Zhang, L.; Gu, X.; Zhang, W.; Zhou, N.; Zhang, Z.; Zhu, X., Sequence-Controlled Polymers with Furan-Protected Maleimide as a Latent Monomer. *Angew. Chem. Int. Ed.* **2017,** *56*, 2328-2333.

17. Launay, K.; Amalian, J.-A.; Laurent, E.; Oswald, L.; Al Ouahabi, A.; Burel, A.; Dufour, F.; Carapito, C.; Clément, J.-L.; Lutz, J.-F.; Charles, L.; Gigmes, D., Precise Alkoxyamine Design to Enable Automated Tandem Mass Spectrometry Sequencing of Digital Poly(Phosphodiester)S. *Angew. Chem. Int. Ed.* **2021,** *60*, 917-926.

18. Leibfarth, F. A.; Johnson, J. A.; Jamison, T. F., Scalable Synthesis of Sequence-Defined, Unimolecular Macromolecules by Flow-Ieg. *Proc. Natl. Acad. Sci.* **2015,** *112*, 10617-10622.

19. Golder, M. R.; Jiang, Y.; Teichen, P. E.; Nguyen, H. V. T.; Wang, W.; Milos, N.; Freedman, S. A.; Willard, A. P.; Johnson, J. A., Stereochemical Sequence Dictates Unimolecular Diblock Copolymer Assembly. *J. Am. Chem. Soc.* **2018,** *140*, 1596-1599.

20. Barnes, J. C.; Ehrlich, D. J. C.; Gao, A. X.; Leibfarth, F. A.; Jiang, Y.; Zhou, E.; Jamison, T. F.; Johnson, J. A., Iterative Exponential Growth of Stereo- and Sequence-Controlled Polymers. *Nat. Chem.* **2015,** *7*, 810-815.

21. Meier, M. A. R.; Barner-Kowollik, C., A New Class of Materials: Sequence-Defined Macromolecules and Their Emerging Applications. *Adv. Mater.* **2019,** *31*, 1806027.

22. Solleder, S. C.; Zengel, D.; Wetzel, K. S.; Meier, M. A. R., A Scalable and High-Yield Strategy for the Synthesis of Sequence-Defined Macromolecules. *Angew. Chem. Int. Ed.* **2016,** *55*, 1204-1207.

23. Hoff, E. A.; De Hoe, G. X.; Mulvaney, C. M.; Hillmyer, M. A.; Alabi, C. A., Thiol–Ene Networks from Sequence-Defined Polyurethane Macromers. *J. Am. Chem. Soc.* **2020,** *142*, 6729-6736.

24. Solleder, S. C.; Schneider, R. V.; Wetzel, K. S.; Boukis, A. C.; Meier, M. A. R., Recent Progress in the Design of Monodisperse, Sequence-Defined Macromolecules. *Macromol. Rapid Commun.* **2017,** *38*, 1600711.

25. Takizawa, K.; Tang, C.; Hawker, C. J., Molecularly Defined Caprolactone Oligomers and Polymers: Synthesis and Characterization. *J. Am. Chem. Soc.* **2008,** *130*, 1718-1726.

26. Koo, M. B.; Lee, S. W.; Lee, J. M.; Kim, K. T., Iterative Convergent Synthesis of Large Cyclic Polymers and Block Copolymers with Discrete Molecular Weights. *J. Am. Chem. Soc.* **2020,** *142*, 14028-14032.

27. Holerca, M. N.; Peterca, M.; Partridge, B. E.; Xiao, Q.; Lligadas, G.; Monteiro, M. J.; Percec, V., Monodisperse Macromolecules by Self-Interrupted Living Polymerization. *J. Am. Chem. Soc.* **2020,** *142*, 15265-15270.

28. Kametani, Y.; Sawamoto, M.; Ouchi, M., Control of the Alternating Sequence for N-Isopropylacrylamide (Nipam) and Methacrylic Acid Units in a Copolymer by Cyclopolymerization and Transformation of the Cyclopendant Group. *Angew. Chem. Int. Ed.* **2018,** *57*, 10905-10909.

29. Teator, A. J.; Varner, T. P.; Knutson, P. C.; Sorensen, C. C.; Leibfarth, F. A., 100th Anniversary of Macromolecular Science Viewpoint: The Past, Present, and Future of Stereocontrolled Vinyl

Polymerization. *ACS Macro Lett.* **2020,** *9*, 1638-1654.

30. Teator, A. J.; Leibfarth, F. A., Catalyst-Controlled Stereoselective Cationic Polymerization of Vinyl Ethers. *Science* **2019,** *363*, 1439-1443.
31. Uchiyama, M.; Satoh, K.; Kamigaito, M., Stereospecific Cationic Raft Polymerization of Bulky Vinyl Ethers and Stereoblock Poly(Vinyl Alcohol) Via Mechanistic Transformation to Radical Raft Polymerization of Vinyl Acetate. *Giant* **2021,** *5*, 100047.
32. Satoh, K.; Kamigaito, M., Stereospecific Living Radical Polymerization: Dual Control of Chain Length and Tacticity for Precision Polymer Synthesis. *Chem. Rev.* **2009,** *109*, 5120-5156.
33. Imamura, Y.; Fujita, T.; Kobayashi, Y.; Yamago, S., Tacticity, Molecular Weight, and Temporal Control by Lanthanide Triflate-Catalyzed Stereoselective Radical Polymerization of Acrylamides with an Organotellurium Chain Transfer Agent. *Polym. Chem.* **2020,** *11*, 7042-7049.
34. Okamoto, Y.; Nakano, T., Asymmetric Polymerization. *Chem. Rev.* **1994,** *94*, 349-372.
35. Ren, J. M.; Lawrence, J.; Knight, A. S.; Abdilla, A.; Zerdan, R. B.; Levi, A. E.; Oschmann, B.; Gutekunst, W. R.; Lee, S.-H.; Li, Y.; McGrath, A. J.; Bates, C. M.; Qiao, G. G.; Hawker, C. J., Controlled Formation and Binding Selectivity of Discrete Oligo(Methyl Methacrylate) Stereocomplexes. *J. Am. Chem. Soc.* **2018,** *140*, 1945-1951.
36. Nishiura, T.; Abe, Y.; Kitayama, T., Uniform Poly(Methyl Methacrylate) Stereostars: Synthesis, Separation and Stereocomplex Formation. *Polym. J.* **2010,** *42*, 868-874.
37. Lengweiler, U. D.; Fritz, M. G.; Seebach, D., Synthese Monodisperser Linearer Und Cyclischer Oligomere Der (R)-3-Hydroxybuttersäure Mit Bis Zu 128 Einheiten. *Helv. Chim. Acta* **1996,** *79*, 670-701.
38. Takizawa, K.; Nulwala, H.; Hu, J.; Yoshinaga, K.; Hawker, C. J., Molecularly Defined (L)-Lactic Acid Oligomers and Polymers: Synthesis and Characterization. *J. Polym. Sci. A, Polym. Chem.* **2008,** *46*, 5977-5990.
39. van Genabeek, B.; Lamers, B. A. G.; de Waal, B. F. M.; van Son, M. H. C.; Palmans, A. R. A.; Meijer, E.

W., Amplifying (Im)Perfection: The Impact of Crystallinity in Discrete and Disperse Block Co-Oligomers. *J. Am. Chem. Soc.* **2017,** *139*, 14869-14872.

40. Nguyen, H. V. T.; Jiang, Y.; Mohapatra, S.; Wang, W.; Barnes, J. C.; Oldenhuis, N. J.; Chen, K. K.; Axelrod, S.; Huang, Z.; Chen, Q.; Golder, M. R.; Young, K.; Suvlu, D.; Shen, Y.; Willard, A. P.; Hore, M. J. A.; Gómez-Bombarelli, R.; Johnson, J. A., Bottlebrush Polymers with Flexible Enantiomeric Side Chains Display Differential Biological Properties. *Nat. Chem.* **2021**, doi: 10.1038/s41557-021-00826-8.
41. Hartweg, M.; Jiang, Y.; Yilmaz, G.; Jarvis, C. M.; Nguyen, H. V. T.; Primo, G. A.; Monaco, A.; Beyer, V. P.; Chen, K. K.; Mohapatra, S.; Axelrod, S.; Gómez-Bombarelli, R.; Kiessling, L. L.; Becer, C. R.; Johnson, J. A., Synthetic Glycomacromolecules of Defined Valency, Absolute Configuration, and Topology Distinguish between Human Lectins. *JACS Au* **2021,** *1*, 1621-1630.
42. Mertens, C.; Soete, M.; Ślęczkowski, M. L.; Palmans, A. R. A.; Meijer, E. W.; Badi, N.; Du Prez, F. E., Stereocontrolled, Multi-Functional Sequence-Defined Oligomers through Automated Synthesis. *Polym. Chem.* **2020,** *11*, 4271-4280.
43. Huang, Z.; Noble, B. B.; Corrigan, N.; Chu, Y.; Satoh, K.; Thomas, D. S.; Hawker, C. J.; Moad, G.; Kamigaito, M.; Coote, M. L.; Boyer, C.; Xu, J., Discrete and Stereospecific Oligomers Prepared by Sequential and Alternating Single Unit Monomer Insertion. *J. Am. Chem. Soc.* **2018,** *140*, 13392-13406.
44. Huang, Z.; Corrigan, N.; Lin, S.; Boyer, C.; Xu, J., Upscaling Single Unit Monomer Insertion to Synthesize Discrete Oligomers. *J. Polym. Sci. A, Polym. Chem.* **2019,** *57*, 1947-1955.
45. Noble, B. B.; Coote, M. L., Chapter Four - Mechanistic Perspectives on Stereocontrol in Lewis Acid-Mediated Radical Polymerization: Lessons from Small-Molecule Synthesis. In *Advances in Physical Organic Chemistry*, Williams, I. H.; Williams, N. H., Eds. Academic Press: 2015; Vol. 49, pp 189-258.
46. Kangani, C. O.; Day, B. W., Mild, Efficient Friedel−Crafts Acylations from Carboxylic Acids Using Cyanuric Chloride and Alcl3. *Org. Lett.* **2008,** *10*, 2645-2648.
47. Arp, F. O.; Fu, G. C., Catalytic Enantioselective Negishi Reactions of Racemic Secondary Benzylic

Halides. *J. Am. Chem. Soc.* **2005,** *127*, 10482-10483.

48. Liu, C.; Pan, B.; Gu, Y., Lewis Base-Assisted Lewis Acid-Catalyzed Selective Alkene Formation Via Alcohol Dehydration and Synthesis of 2-Cinnamyl-1,3-Dicarbonyl Compounds from 2-Aryl-3,4-Dihydropyrans. *Chin. J. Catal.* **2016,** *37*, 979-986.
49. Boros, S.; Gáspári, Z.; Batta, G., Chapter One - Accurate Nmr Determinations of Proton–Proton Distances. In *Annual Reports on NMR Spectroscopy*, Webb, G. A., Ed. Academic Press: 2018; Vol. 94, pp 1-39.
50. G M Clore, a.; Gronenborn, A. M., Two-, Three-, and Four-Dimensional Nmr Methods for Obtaining Larger and More Precise Three-Dimensional Structures of Proteins in Solution. *Ann. Rev. Biophys. Biophys. Chem.* **1991,** *20*, 29-63.
51. Wunderlich, B., Reversible Crystallization and the Rigid–Amorphous Phase in Semicrystalline Macromolecules. *Prog. Polym. Sci.* **2003,** *28*, 383-450.
52. Xu, W.-S.; Douglas, J. F.; Sun, Z.-Y., Polymer Glass Formation: Role of Activation Free Energy, Configurational Entropy, and Collective Motion. *Macromolecules* **2021,** *54*, 3001-3033.
53. White, R. P.; Lipson, J. E. G., Polymer Free Volume and Its Connection to the Glass Transition. *Macromolecules* **2016,** *49*, 3987-4007.
54. Natta, G.; Corradini, P., Conformation of Linear Chains and Their Mode of Packing in the Crystal State. *J. Polym. Sci.* **1959,** *39*, 29-46.
55. Liu, R.; Yang, C.; Huang, Z.; French, R.; Gu, Z.; Cheng, J.; Guo, K.; Xu, J., Unraveling Sequence Effect on Glass Transition Temperatures of Discrete Unconjugated Oligomers. *Macromol. Rapid Commun.* **2021,** *42*, 2100666.
56. Xu, X.; Douglas, J. F.; Xu, W.-S., Influence of Side-Chain Length and Relative Rigidities of Backbone and Side Chains on Glass Formation of Branched Polymers. *Macromolecules* **2021,** *54*, 6327-6341.

Graphic Abstract